HHS Public Access

Author manuscript

J Tissue Eng Regen Med. Author manuscript; available in PMC 2019 June 01.

Published in final edited form as:

J Tissue Eng Regen Med. 2018 June ; 12(6): 1389–1401. doi:10.1002/term.2669.

Electrophysiological Assessment of a Peptide Amphiphile Nanofiber Nerve Graft for Facial Nerve Repair

Jacqueline J Greene, MD[1], **Mark T. McClendon, PhD**[2,3], **Nicholas Stephanopoulos, PhD**[2,3], **Zaida Álvarez, PhD**[2,3], **Samuel I. Stupp, PhD**[2,3,4,5], and **Claus-Peter Richter, MD, PhD**[1,5,6,7]

[1]Department of Otolaryngology-Head and Neck Surgery, Northwestern University, Feinberg School of Medicine, Chicago, IL 60611, USA

[2]Simpson Querrey Institute for BioNanotechnology Northwestern University, Evanston, IL 60208, USA

[3]Department of Materials Science and Engineering, Northwestern University, Evanston, IL 60208, USA

[4]Department of Chemistry, Northwestern University, Evanston, IL 60208, USA

[5]Department of Medicine, Northwestern University, Evanston, IL 60208, USA

[6]Department of Biomedical Engineering, Northwestern University, Evanston, IL 60208, USA

[7]The Hugh Knowles Center, Department of Communication Sciences and Disorders, Northwestern University, Evanston, Illinois, U.S.A

Abstract

Facial nerve injury can cause severe long-term physical and psychological morbidity. There are limited repair options for an acutely transected facial nerve not amenable to primary neurorrhaphy. We hypothesize that a peptide amphiphile nanofiber neurograft may provide the nanostructure necessary to guide organized neural regeneration. Five experimental groups were compared, animals with 1) an intact nerve, 2) following resection of a nerve segment, and following resection and immediate repair with either a 3) autograft (using the resected nerve segment), 4) neurograft, or 5) empty conduit. The buccal branch of the rat facial nerve was directly stimulated with charge balanced biphasic electrical current pulses at different current amplitudes while nerve compound action potentials (nCAPs) and electromygraphic (EMG) responses were recorded. After 8 weeks, the proximal buccal branch was surgically re-exposed and electrically evoked nCAPs were recorded for groups 1-5. As expected, the intact nerves required significantly lower current amplitudes to evoke an nCAP than those repaired with the neurograft and autograft nerves. For other electrophysiologic parameters such as latency and maximum nCAP, there was no significant difference between the intact, autograft and neurograft groups. The resected group had variable

Corresponding author: Dr. Jacqueline J Greene, 243 Charles Street, Boston, MA 02114, Phone: 617-573-3641, Fax: 617-573-3727, jacqueline_greene@meei.harvard.edu.

**NS present address: School of Molecular Sciences, Biodesign Center for Molecular Design and Biomimetics, Arizona State University, Tempe, Arizona 85287

Conflict of Interest: Coauthors JG, MM and SS are in the process of patent submission.

Level of Evidence: NA, animal study

responses to electrical stimulation, and the empty tube group was electrically silent. Immunohistochemical analysis and TEM confirmed myelinated neural regeneration. This study demonstrates that the neuroregenerative capability of peptide amphiphile nanofiber neurografts is similar to the current clinical gold standard method of repair and holds potential as an off-the-shelf solution for facial reanimation and potentially peripheral nerve repair.

Keywords

Facial Nerve Repair; Nanofiber Neurograft; electrophysiology; Neural Regeneration

1. Introduction

Facial paralysis causes devastating physical and psychological morbidity. It can result from trauma, iatrogenic injury during routine surgery, Bell's Palsy and other medical disorders. Paralysis also occurs after the nerve has been intentionally sacrificed during a parotid cancer resection (Bron & O'Brien, 1997; Jowett & Hadlock, 2015; Ridgway et al, 2015). The facial nerve is the 7th cranial nerve and exits from the stylomastoid foramen on the infero-lateral aspect of the skull. The facial nerve has been reported to have 4650 myelinated axons in the main trunk and 1955 myelinated axons in the buccal branch in rats(Mattox & Felix, 1987). Facial paralysis can lead to many secondary complications, including blindness from exposure keratitis due to incomplete eye closure, external nasal valve collapse, oral incompetence, and difficulty expressing facial emotions (Hadlock et al, 2011; Iseli et al, 2010). Facial nerve transection is ideally repaired with end-to-end tensionless microsurgical repair. However, if this is not possible due to the size of the gap between proximal and distal nerve ending, repair options are limited and typically involve autografting, which requires the harvest of a donor nerve from elsewhere in the body (Biazar et al, 2010; Boahene, 2013; Iseli et al, 2010; Jowett & Hadlock, 2015). Disadvantages of autografting include donor site morbidity, increased surgery time, possible cross-contamination in cancer patients, as well as donor nerve length/diameter mismatch with the recipient nerve stump. Other facial reanimation procedures can be beneficial but may have specific disadvantages such as unnatural facial movements while speaking or chewing (hypoglossal or masseteric nerve transfers) or dynamic asymmetry from single vector reanimation (temporalis tendon transfer or gracilis free tissue transfer) (Hadlock et al., 2004; Jowett & Hadlock, 2015; Kochhar et al., 2016; Owusu et al, 2016; Sidle & Fishman, 2011)). Current surgical interventions for facial reanimation after a complete facial nerve transection do not return full function, (at best, House-Brackmann III where the eyelid can close but there is an obvious facial asymmetry and dysfunction, (Biazar et al, 2010; Iseli et al, 2010)). Time delays to assess for facial nerve recovery can cause prolonged denervation leading to distal muscular atrophy and decreased capacity of Schwann cells to remain in the pro-regenerative state. Those delays ultimately contribute to incomplete neural regeneration (Allodi et al, 2012).

A synthetic nerve graft would provide an off-the-shelf solution for a transected facial nerve not amenable to primary repair. Benefits would include obviating the need for donor nerve harvest, eliminating the risk of cross-contamination during cancer resection, reducing the number of reconstructive surgeries, and thereby accelerating the time for return of facial

movement and function. Although there are a few commercially available peripheral nerve grafts, they are not routinely used in Otolaryngology clinical practice for facial nerve repair, due to cost and poorer performance than autografting, although this may differ among specialties, and the cost and donor morbidity of autografting also should be considered(Brattain, Medical, & Consultants, 2013). Commercially available, FDA approved peripheral nerve guide conduits include polyglycolic acid tubes (Neurotube®, Synovis), poly DL-lactide-ε-caprolactone tubes (Neurolac®, Ascension Orthopedics), and type I collagen tubes (NeuraGen®, Integra Life Sciences Corp. and Neuroflex® and Neuromatrix®, Collagen Matrix Inc) (Bell & Haycock, 2012; Biazar et al, 2010; Kehoe et al, 2012). The challenge for synthetic neurografts is the mechanism and efficacy of the approach. Prior studies in the rat facial nerve with empty tube repair have not shown clinically meaningful recovery even for an appropriate nerve gap and time frame, which is normally needed for axonal regeneration. The empty tube repair of a 2 mm defect of a rat facial nerve (main trunk and peripheral branches) led to minimal whisking recovery after 4 months due to severe axonal misrouting which has been identified from histology (Hadlock et al, 2010). Allografts such as the decellularized cadaveric peripheral nerves (Avance nerve graft®, AxoGen Inc) or the porcine small intestinal submucosa (AxoGuard Nerve Connector®, Cook Biotech Products) (Bell & Haycock, 2012; Kehoe et al, 2012) are available with possible but low infectious and immunologic risks. Moreover, the grafts have not been shown to perform better than autologous tissue (Whitlock et al, 2009).

Here we present a novel approach. Nanofiber hydrogels may provide the topographic guidance necessary for the actively regenerating neural growth cone to elongate as well as promote a surface upon which Schwann cells can re-myelinate (Daly et al, 2012) and form the bands of Büngner that guide organized axonal regeneration (Allodi et al, 2012). Confocal imaging of a nerve transection revealed the regenerating axonal sprouts diameters are on the order of 10 μm or less (Grinsell & Keating, 2014), whereas TEM of the rat facial nerve in one study measured the average myelinated axon diameter to be 5 μm (Cao et al, 2013). Recently, it has been demonstrated that the peptide amphiphile (PA) nanofibers (~6-8 nm in diameter) can be aligned into a single, macroscopic noodle-like hydrogel several millimeters in diameter, with length reaching several centimeters while retaining a high degree of alignment down to the nanoscale. These noodle gels were shown to direct axon growth parallel with the fiber axis *in vitro* (Berns et al, 2014; Zhang et al, 2010). In a separate study, aligned PA nanofiber constructs within a polymer conduit were implanted into rat sciatic nerves and found to improve walking and paw reflexes, as well as neural regrowth on histology (Li et al, 2014). However, no electrophysiologic studies or transmission electron microscopy were completed.

This study investigates the neuroregenerative capability of the aligned PA nanofiber neurograft for facial nerve repair in an *in vivo* rat model through quantitative electrophysiological characterization via direct neural stimulation. Aligned nanofiber neurografts containing only PA nanofibers were constructed within a type I collagen external tube and anastomosed via clinically relevant microsurgical techniques to repair a defect of the rat facial nerve. Eight weeks after the surgery, the nerve compound action potentials (nCAP) of the neurografted rat facial nerve was compared to intact, resected nerves and

those repaired with an autograft or empty tube. An *in vitro* study of seeded motor neuronal cells on an aligned nanofiber surface was also completed.

2. Materials and Methods

2.a. Peptide Amphiphile Nanofiber Neurograft Preparation

Peptide amphiphile (PA) molecules with the amino acid sequence palmitoyl-VVVAAAEEE were synthesized and purified according to previously reported protocols, and stored as a lyophilized powder at −20°C (Berns et al, 2014). For gel construction, PA was solubilized to a concentration of 10 mg/ml in PBS, heated at 80°C in a water bath for 30 min and cooled to room temperature overnight. Aligned nanofibers were formed inside type I collagen tubes (purchased from Neuragen®, Integra Life Sciences Corp., 1.5 mm inner diameter) by flowing heat-treated PA nanofibers through a 40 μm pore size mesh into the type I collagen tube, followed by immersing the tube in a 25 mM $CaCl_2$ bath for 2 h (Figure 1a). During the gelation process, the nanofibers become ionically crosslinked, thereby locking the alignment in place as visualized by scanning electron microscopy (Figure 1d). The resulting neurografts were cut into 7.5 mm lengths (Figure 1b) and kept sterile.

2.b. Animal Surgery

All animal procedures were carried out in accordance with the NIH Guide for the Care and Use of Laboratory Animals and were approved by the Institutional Animal Care and Use Committee at Northwestern University.

Adult female Sprague-Dawley rats (200-230g, Charles River Laboratories) were randomly assigned to five experimental groups of 6 animals each (see below). The animals were anesthetized with an initial induction 3-4% inhaled isoflurane and maintained with 1-3% inhaled isoflurane. The level of anesthesia was monitored continuously using the electrocardiogram (EKG) and the paw withdrawal reflex. Vitals were recorded every 15 minutes. After the surgical area was prepared in a sterile fashion, an approximately 2.5 cm curvilinear incision was made from the mastoid to the lateral buccal region. The parotid gland was carefully elevated and the buccal and marginal mandibular branches of the facial nerves were exposed and released from surrounding tissue. The buccal branch of the rat facial nerve was 1) left intact (N=6), 2) resected (7.5 mm segment; N=6), 3) autografted (resected a 7.5 mm segment, reversed to prevent synkinesis as typically performed clinically then immediately repaired with the resected nerve segment; N=6), 4) neurografted (resected followed by repair with the PA nanofiber neurograft; N=6), or 5) resected and repaired with an empty tube (N=6) (Figure 2a-d). All neural anastomoses were completed using 2-3 epineural stitches with 9-0 ethilon under microscopic or loupes visualization utilizing microsurgical instruments. Primary closure of the skin incision was obtained via a subcuticular running closure with 4-0 Vicryl suture. Following electrical testing 8 weeks after surgical intervention, the animals were sacrificed and the facial nerves were harvested for histologic examination.

2.c. Electrophysiological Testing

Two forms of electrophysiological testing were used in this study- evoked electromyography (EMG) and direct neural stimulation (Cao et al., 2013; Claudel, A, Lazaro, RT, Wolfe, G, Adams, 2016; Davis, LA, Gordon, TJ, Hoffer, JA, Jhamandas, J, Stein, 1978; Goodnight, Dulguerov, Berke, Lesavoy, & Hoffman, 1995).

Evoked electromyography (EMG) was performed during the first surgery (t=0) to provide baseline data and 8 weeks after the manipulation of the facial nerve. To evoke the nerve compound action potential, biphasic (250 μs/phase) charge balanced electrical pulses were delivered with a bipolar stimulating electrode to the proximal buccal branch of the facial nerve in alternating phase at increasing current amplitudes between 0 and 1.4 mA at steps of 0.1 mA. The resulting muscle compound action potentials (mCAPs) were recorded with an electrode inserted into the orbicularis oris muscle.

Direct neural stimulation was performed through a single electrical stimulation and recording electrode was used directly on the buccal branch of the facial nerve (Figure 3a). Care was taken to ensure the nerve was completely dissected from surrounding soft tissue and elevated freely above the plane of the rat musculature (Figure 3a). The nerve was kept moist with saline drops every 15 minutes throughout surgery. The onset of the stimulus occurs at 5 milliseconds (ms). Electrical current stimuli were biphasic pulses as described for the mCAPs above. The evoked nCAP was measured with the recording electrode located 7.5 mm distal to the stimulus electrode (Figure 3a). The measured voltage was filtered (300 Hz to 3 kHz) and amplified 1000 times by an electrode amplifier (ISO80, World Precision Instruments, Sarasota, FL). nCAPs were recorded at each current level with a 12 bit computer analog-to-digital board (KPCI-3116, Keithley, Cleveland, OH) at a 50 kHz sampling rate. The averaged responses to 20 stimulus presentations for each stimulus condition was stored. The results were analyzed off-line with Igor Pro (WaveMetrics version 4.0, Lake Oswego, OR) by plotting the nCAP versus time at each current amplitude for each animal.

An electrical artifact was noted immediately following the onset of electrical stimulus at 5 ms (Figure 3b). From the traces the following electrophysiologic parameters were determined: threshold current necessary to elicit a nCAP, latency between the onset of the stimulus and the first peak (at threshold and maximum stimulation currents), maximum nCAP, were measured with Igor Pro (WaveMetrics version 4.0, Lake Oswego, OR) (Figure 3b).

2. d. Immunohistochemical Analysis

At the conclusion of the study (8 weeks following surgical exposure of the facial nerve), the rats were euthanized with Euthasol (pentobarbital sodium and phenytoin sodium) followed by decapitation. The autograft, neurograft and empty tube samples were harvested from the central portion (between suture marks, ensuring no native neural tissue was included). For the resected nerve group, a portion of the distal stump of the buccal branch of the facial nerve was harvested. The nerve specimens were fixed in 10% neutral buffered formalin for

at least 48 h, embedded in paraffin, deparaffinized and sectioned (4 μm thickness). Select slides were stained with conventional hematoxylin-eosin.

Immunohistochemical analysis was also performed. Endogenous peroxidase was blocked with 3% hydrogen peroxidase in ddH_2O. Endogenous biotin was blocked with avidin and all non-specific proteins were blocked with 5% normal donkey serum. Mouse monoclonal antibody to rat neurofilament (anti-NF, 1:250 dilution, Abcam, Cambridge, MA) and rabbit polyclonal antibody to rat S-100 (1:500 dilution, Sigma Aldrich, St. Louis, MO) were applied overnight respectively. The slides were incubated with a biotinylated antibody followed by the Vectastain ABC kit (Vector laboratories) and then incubated with Biotinyl Tyramide working solution. The signal was detected using streptavidin horseradish peroxidase and visualized with diaminobenzidine (DAB) reaction. The sections were counterstained with hematoxylin. Positive and negative controls for immunohistochemical analysis were completed.

2.e. Transmission Electron Microscopy

Intact neural tissue, as well as samples from the center of the neurograft, autograft, and a portion of the distal stump of the facial nerve from the resected group were harvested and fixed in 2% paraformaldehyde and 2.5% glutaraldehyde in 0.1 M sodium cacodylate buffer pH 7.3 and post-fixed with unbuffered 2% osmium tetroxide, rinsed with distilled water, en bloc stained with 3% uranyl acetate, rinsed with distilled water, dehydrated in ascending grades of ethanol, transitioned with propylene oxide and embedded in resin mixture from Embed 812 kit, cured in a 60°C oven. Samples were sectioned on a Leica Ultracut UC6 ultramicrotome. 1 μm thick sections were collected and stained with Toluidine Blue O and 70 nm sections were collected on 200-mesh grids; thin sections were stained with uranyl acetate and Reynolds lead citrate. Thin sections were examined on FEI Tecnai Spirit G2 TEM, and digital images were captured with an FEI Eagle camera. Samples were processed by the Center of Advanced Microscopy at Northwestern University Feinberg School of Medicine. Myelin thickness, axon count and diameter were measured using ImageJ from images taken at 690× magnification using the automated analyze particle function for the intact, resected, autograft and neurograft groups. Axon count density was measured and normalized per 1000 μm^2. Myelin thickness was calculated by automatically tracing the inner and outer diameter of the myelin sheath and taking the difference.

2.f. In vitro culture of motor neural cells with aligned nanofibers

Motor neurons were obtained from embryonic spinal cords, as described (Graber & Harris, 2013). Briefly, a time pregnant mouse was sacrificed by cervical dislocation and the embryos were extracted at embryonic day 18 (E18). Spinal cords were dissected free of meninges in a solution of PBS with 0.6% glucose (Sigma-Aldrich), 0.3% BSA (Sigma-Aldrich) and digested with trypsin (Biological Industries) DNAse I (Sigma-Aldrich) for 10 min at 37°C. The tissue was mechanically dissociated, centrifuged and resuspended in CO_2-equilibrated Leibovitz's L-15 medium (L-15) supplemented with 10% NHS, 1% Pen-Strep, 0.5 mM L-Glutamine, 5.8 μl/ml NaHCO3 (Sigma-Aldrich). Cells were separated by density gradient centrifugation using OptiPrep Density gradient Medium (Sigma Aldrich). The layered tube was centrifuged for 15min at 4°C. The supernatant was decanted and the pellet

was resuspended in 1 mL of freshly prepared motor neuron growth medium (NB, 1%NHS, 1% Pen-Strep, 0.5 mM L-glutamine, 22 μM glutamic acid (Sigma-Aldrich), 2% B27 (Gibco), 5.8μl/ml NaHCO3) and plated at a density of 2.5×10^5 cells/cm^2 directly on aligned nanofiber surfaces. Aligned nanofiber surfaces were prepared by dragging a glass surface over the annealed PA solution and immediately gelling the PA nanofibers by exposure to a 25 mM $CaCl_2$ solution. After seeding cells onto the aligned nanofibers they were cultured for 5 days then fixed in a 3% glutaraldehyde solution for 20 min and prepared for SEM.

2.g. Scanning Electron Microscopy (SEM)

For imaging by scanning electron microscopy, samples were dehydrated in a series of ethanol/water washes of subsequently increasing ethanol concentration (30%, 40%…100%). When samples reached 100% EtOH they were then critically point dried in using an automated Samdri®-795 (Tousimis), mounted with carbon adhesive tape, and coated with approximately 8 nm of osmium before being imaged using a LEO Gemini 1525 sFEG SEM instrument.

2.h. Data Analysis

Current amplitude versus threshold plots were variable. To better demonstrate the differences among groups we also plotted the data using cumulative plots. The fraction of animals, which had a threshold current value to stimulate the facial nerve equal or smaller to a selected current amplitude were summed. The range for the current amplitude was between 0 and 1.4 mA. The cumulative plot increases in a sigmoidal fashion from 0 (below threshold) to 1 (all animals showed a response at this current level). Figure 7a shows the data as the lines with the markers. The fit of the following equation, $base+\{max/(1+\exp((xhalf-x)/rate))\}$, is shown by the broken line. For the fitting the following parameters have been fixed: base=0 and max=1. *xhalf* is the current amplitude *x* for *f(x)*=0.5 and the rate describes the growth of the function. A shift of the curve to the right indicates an increase in threshold. A decrease of the maximum value below 1 indicated that a response could not be evoked in all of the animals (Fig 7a). Multiplying the results by 100 provides the values in %. Curve fitting accomplished with a routine in Igor Pro (WaveMetrics version 4.0, Lake Oswego, OR).

2.i. Statistical Analysis

A one-way analysis of variance (ANOVA) was used to compare electrophysiologic parameters using R Statistical Package version 3.2.3 (2015-12-10). The Bonferroni post-hoc multi-comparison adjustment was used to calculate significance levels. $p < 0.05$ was considered statistically significant.

3. Results

3.a. Evoked Electromyography

The evoked electromyography data was limited in that the mCAP of the intact and resected nerves after 8 weeks had similar threshold currents, rendering it difficult to distinguish between these controls (Figure 4a-b). Given the similarity in threshold currents in intact and

resected nerves using evoked EMG, a more sensitive method for functional testing was undertaken, direct neural stimulation (Fig 4c-d).

3.b. Direct Neural Stimulation

Direct neural stimulation elicited nCAPs by stimulating and recording directly from the buccal branch of the facial nerve through a single electrical stimulation and recording electrode (Figure 2a). A comparison of evoked EMG and direct neural stimulation is shown in Figure 4 where the mCAPs and nCAPs of intact and resected nerves after 8 weeks are recorded. The threshold to nCAPs of the intact nerve generally occurred at a current <0.1 mA (Figure 4c), whereas the resected nerves after 8 weeks required a higher threshold current to stimulation or were electrically silent (Figure 4d), and thus were more readily distinguishable than through EMG.

Compound Nerve Action Potentials—Figure 5 demonstrates typical examples of individual nCAPs for the different experimental groups. Selected current amplitude values were 0.1, 0.5 and 1.0 mA for a) intact nerves, and 8 weeks following b) resection, c) autograft repair, d) neurograft repair, and e) repair with an empty tube. Each group was composed of 6 rats. The electrical artifact at 5 ms indicates the current onset (as demonstrated in Fig 3b). As described in the Methods, from these traces the threshold current, the maximum nCAP amplitude, latency at threshold current, and latency at the maximum nerve action potential for the intact, autograft, neurograft, resected and empty tube groups were determined (Figure 6a-f).

Threshold for stimulation—Intact nerve thresholds were significantly lower on average 0.1±0.06 mA than the autograft on average 0.56±0.2 mA, ($F(2,15)=15.19$, $p=0.0006$) or neurograft groups on average 0.55±0.18 mA, ($F(2,15)=15.19$, $p=0.0009$) (Figure 6a). There was no significant difference in threshold between the autograft and neurograft groups. The resected group had 4 of the 6 nerves stimulate for thresholds shown in Figure 6a, however an average could not be taken as 2 nerves were electrically silent. The threshold currents for the resected group ranged from 0.4-0.7 mA. The repair with empty tube were electrically silent. Experimental groups were tested 8 weeks following autograft repair and neurograft repair.

Maximum nCAP amplitude—The maximum nCAP (Figure 6b) was measured peak-to-peak for the different experimental groups and was variable; 2.23±1.3 mV for the intact nerve group, 2.28±1.6 mV for the autograft group, and 0.90±0.4 mV for the neurograft group. There was no significant difference between the intact, autograft and neurograft groups.

The number of animals in the groups with intact and resected nerves that produced a nCAP at currents ranging from 0-1.2 mA is depicted in Figure 7a, with curve fitting, the threshold shift is revealed. In this study only 60% of the resected nerve group produced a nCAP even at the highest current amplitude tested, whereas 0% of the empty tube group produced a nCAP (electrically silent). The percentage of all groups producing a nCAP across tested currents is shown in Figure 7b.

3.c. Immunohistochemical Analysis

Neural continuity and phenotype of the intact facial nerve buccal branch was demonstrated as expected through cross-sections stained with H&E, anti-Neurofilament (NF), and anti-S100 (Figure 8a). The distal end of the buccal branch of the facial nerve that had been resected 8 weeks prior demonstrated intact neural phenotype as well.

Neural regeneration from the proximal buccal branch of the facial nerve through the autograft and neurograft is likewise confirmed (Figure 8a). A cross-sectional view of the entire neurograft and empty tube samples are shown in Figure 8b, demonstrating the robust neural regeneration across the neurograft and relative paucity of neural tissue across the empty tube control.

3.d. Transmission Electron Microscopy (TEM)

TEM imaging of cross-sections of the intact, resected distal stump, autograft and neurograft tissues are shown (Figure 9a top). A more detailed view is shown (Figure 9a bottom) revealing myelin layers encasing individual axons of the intact nerve, and in thinner, more irregular layers for the autograft group. Robust myelinated axonal regeneration for the neurograft is likewise visualized through the TEM cross-section (Figure 9a). The resected nerve distal stump shows paucity of axonal tissue, disorganized remaining axons, and degenerating myelin layers.

Average myelin thickness of the intact nerve (Figure 9b) was significantly greater than the resected and autograft groups (4.1±0.9 μm, 1.4±0.5 μm, 1.7±0.6 μm, p=3.1e-10, p=4.2e-9, respectively). The neurograft myelin thickness (4.3±0.7 μm) was significantly also significantly greater than the resected and autograft groups (p=4.0e-11, p=4.9e-10, respectively). No significant different in myelin thickness was found between the neurograft and intact groups (p=0.9). Average axon diameter of the intact nerve (Figure 9b) was significantly greater than the resected and autograft groups (9.7±2.1 μm, 3.6±0.9 μm, 4.2±1.5 μm, p=5.5e-10, p=6.0e-9, respectively). The neurograft axon diameter (12.6±1.8 μm) was significantly also significantly greater than the resected and autograft groups (p=4.7e-13, p=5.1e-13, respectively). The neurograft axon diameter was also significantly greater than the intact nerve (p=0.0008). Axon count density was highest in the autograft group (39.3 axons/1000μm^2), followed by the intact group (19.5 axons/1000μm^2), neurograft (14.6 axons/1000μm^2), and lastly the resected group (10.4 axons/1000μm^2).

3.e. Scanning Electron Microscopy (SEM) imaging of in vitro motor neuron culture with aligned PA nanofibers

Figure 10 demonstrates SEM imaging which captured *in vitro* motor neurons extending along the axis of the aligned nanofibers, suggesting a possible mechanism by which the aligned nanofibers guide neural regeneration.

4. Discussion

This is the first direct neural electrophysiological analysis of the peptide amphiphile nanofiber neurograft for facial nerve repair in an animal model and successfully

demonstrates that there was no statistical difference between autograft and neurograft repair, indicating similar degrees of neural regeneration and recovery between these two repair techniques. Furthermore, there was no statistically significant difference between the intact, autograft, and neurograft groups for compound nerve action potential, or peak or threshold latency after 8 weeks. Clinically for facial paralysis patients, this would mean that although there would still likely be asymmetry following repair of a transected facial nerve by autografting or neurografting due to higher thresholds, emotive facial movement such as a smile or blink would occur at a similar delay time, speed and strength as the non-injured side. This study is in agreement with a recent study (Li et al., 2014), which demonstrated improved behavioral responses (latency to hindpaw withdrawal from a thermal stimulus and gait patterns) after sciatic nerve resection and neurograft repair but provided no electrophysiological data. We also used evoked EMG to assess the neurograft, but found within our experimental schema where the resected nerve ends were not ligated, the mCAP did not change significantly enough after nerve resection to readily distinguish between controls (Figure 4). The length of study (8 weeks) was chosen to capture optimal neural regeneration, but also reveal any potential degenerative changes. Under ideal conditions, neural regeneration growth occurs at a rate of 1 mm /day (Arslantunali et al, 2014), and so regeneration should ideally occur within 7-8 days for a 7.5 mm gap. Extensive studies by Hadlock et al have demonstrated that after nerve transection, changes to rat whisking amplitude and distal muscle atrophy are seen at 8 weeks (Hadlock et al., 2013). Moreover, Banks et al demonstrated that functional whisking recovery from a single nerve transection and immediate neurorrhaphy repair remains similar from 4 weeks to as far as 6 months (Banks et al., 2015).

While human facial nerve studies tend to rely on subjective grading scales such as House-Brackmann (Albathi et al., 2015; Iseli et al., 2010), functional grading schema have been used to describe rat facial nerve function (whisker movement (Banks et al., 2015; Cao et al., 2013), blink reflex (Hadlock et al, 2005)). One disadvantage of these methods often require implanted head fixation devices that can extrude or become infected and reflect the entire neuromuscular pathway for facial movement similar to evoked EMG (Banks et al., 2015; Hadlock et al., 2005; Hadlock et al, 2001; Hohman et al., 2014). In the clinical setting, evoked electromyography can be used to assess posttraumatic or idiopathic acute onset facial paralysis (Biglioli et al., 2012; Flint, 2015), however few studies provide electrophysiological data to evaluate neural regeneration. Direct nerve stimulation was chosen for this study in order to isolate and quantify the electrophysiological profile of an individual branch of the regenerating facial nerve. It was termed direct neural stimulation as the stimulating and recording electrodes are set at a fixed distance using the same two-prong tool while gently elevating the nerve above the surrounding tissue (Figure 2a). This electrode design allowed for exact measurement of a variety of parameters (Figure 2b). Intact direct nerve thresholds are lower (0.1±0.06 mA) than those previously reported for evoked EMG (0.26±0.13 mA), but remain comparable to other studies reported evoked EMG thresholds for the buccal facial nerve (0.3 mA in a single rabbit (Goodnight et al, 1995)).

In this study, it was difficult to quantify the resected and empty tube groups given some nerves partially recovered and some were electrically silent; individual data points for all rats involved even if electrically silent were included in order to demonstrate the variability

in neural recovery, or lack thereof (circled data points in Figure 6). The threshold shift from the intact to resected groups in Figure 7 readily demonstrate how similarly autografting and the neurografts perform, and concurs with the clinical finding that no method of repair for a complete neural resection leads to a complete recovery (Biazar et al., 2010; Iseli et al., 2010). In this study, improved neural recovery were found in the resected group as compared to the empty tube group in that 4 of the 6 resected rat nerves were electrically stimulatable while 2 were electrically silent, as compared to the empty tube group which were universally electrically silent. The neural regeneration of some of the resected rat nerves is most likely due to the fact that the resected nerve ends were not suture-ligated or prevented from local reinnervation. In contrast to human facial nerve anatomy with distinct areas of facial innervation, cross-innervation to the whisker pad in the rat have been well documented. Henstrom et al demonstrated that minimal change in rat whisking occurred 3 days following isolated buccal or mandibular branch transection, but that transection of both branches led to elimination of whisking (Henstrom et al., 2012). One study did report that a transected rat facial nerve trunk did produce CMAPs, albeit at a significantly slower latency and conduction velocity compared to the intact nerve (Byrne et al, 2005). The paucity of neural ingrowth into the empty tubes on histology (Figure 8b) correlates with the electrical silence after 8 weeks (Figure 6), as the amplitude of a compound nerve action potential is generally related to the number of axons available for stimulation (Claudel et al, 2016).

This is also the first report of organized, myelinated neural regeneration through an aligned PA nanofiber neurograft (Figure 9) in the rat facial nerve. Previous studies have demonstrated neural regeneration through a PA nanofiber neurograft in the rat sciatic nerve (Li et al., 2014) and the cavernous nerve (Angeloni et al., 2011; Bond et al., 2011; Choe et al., 2018) although electrophysiological testing was not performed. The myelin sheath surrounds each axon, is produced by Schwann cells, and acts as a capacitor, greatly contributing to the conduction velocity of peripheral nerves (Claudel et al, 2016). Other measurements based on histology and TEM such as axon count or density was avoided due to the risk for selection bias, but clear differences between the disorganized sparsely populated distal stump of the resected nerve and the intact, autograft and neurograft groups can be seen (Figure 9). *In vitro* culture of mouse motor neurons with the aligned PA demonstrate directed growth extending along the aligned PA nanofibers within 5 days (Figure 10), although it is recognized that the embryonal mouse motor neurons may function differently than aged neurons *in vitro* and *in vivo*.

A synthetic neurograft that performed as well as autografting could decrease surgical times of harvesting the donor nerve, donor site morbidity, prevent potential cross-site contamination in cancer resection surgeries, and potentially decrease the number of reconstructive surgeries for facial paralysis. Previously reported synthetic alternatives to autografts are limited, expensive and outcomes generally show some promise for short gaps (less than 20 mm) but remain inferior to autografting (Bell & Haycock, 2012). Prior studies of synthetic neurografts indicated that neurografts are limited by inefficient neural regrowth (Bailey et al, 1993), axonal degeneration (Le Beau et al, 1988), lack of Schwann cell proliferation (Daly et al., 2012), disordered or thin myelin sheaths or require exogenous neurotrophic factors to regenerate (Cao et al., 2013), scar infiltration, poor mechanical support, and chronic inflammation from synthetic materials (Daly et al., 2012). Many of the

studies come from the Orthopedic Surgery and Neurology literature with studies of the rat sciatic nerve and tube conduits (Kehoe et al., 2012; Shin et al, 2009). One study compared repair of a 10 mm sciatic nerve defect in rats with autografting, Neurolac®, NeuraGen® and Neurotube® and found no significant difference in compound muscle action potential after 12 weeks. However the reported CMAP variation was large and no values for an intact and resected nerve were reported (Shin et al., 2009). In this study, empty tube repair led to minimal neural regrowth after 8 weeks and electrical silence for a 7.5 mm nerve gap. The addition of PA nanofibers to the neurograft without additional neurotrophic factors or cells led to myelinized neural regeneration and comparable electrophysiological recovery as autografting, likely due to the aligned nanostructure conducive to organized neural regeneration.

5. Conclusion

This is the first direct neural electrophysiological analysis of the peptide amphiphile nanofiber neurograft for facial nerve repair in an animal model and successfully demonstrates similar immunohistochemical, structural and electrophysiological regeneration between the current clinical gold standard, autografting, and neurograft repair. This is also the first report of organized, myelinated neural regeneration through the PA nanofiber neurograft. The PA nanofiber neurograft can serve as an off-the shelf option for facial nerve transection not amenable to end-to-end tensionless microsurgical repair.

Acknowledgements

The authors are especially grateful for the technical support and expertise of Lennell Reynolds (Northwestern University Center for Advanced Microscopy generously supported by NCI CCSG P30 CA060553 awarded to the Robert H Lurie Comprehensive Cancer Center), Dr. Lin Li (Mouse Histology and Phenotyping Laboratory, Northwestern University) and Hunter Young (laboratory manager, Richter lab, Northwestern University).

Research reported in this publication was supported, in part, by the American Academy of Facial Plastic and Reconstructive Surgery Foundation Leslie Bernstein Grant, and the National Institutes of Health's National Center for Advancing Translational Sciences, Grant Number UL1TR000150, as administered by the Northwestern University Clinical and Translational Sciences Institute (NUCATS) pilot grant program. Z.A. received postdoctoral support from the Beatriu de Pinós Fellowship 2014 BP-A 00007 (Agència de Gestió d'Ajust Universitaris i de Recerca, AGAUR) and the PVA Grant # PVA17_RF_0008 from the ParalyzedVeterans of America (PVA) Research Foundation. S. I. S. research was supported by the Northwestern University Center for Regenerative Nanomedicine through a CRN Catalyst Award. The content is solely the responsibility of the authors and does not necessarily represent the official views of the National Institutes of Health.

REFERENCES

Albathi M, Oyer S, Ishii LE, Byrne P, Ishii M, & Boahene KO (2015). Early Nerve Grafting for Facial Paralysis After Cerebellopontine Angle Tumor Resection With Preserved Facial Nerve Continuity. JAMA Facial Plastic Surgery, 21287, 1 https://doi.org/10.1001/jamafacial.2015.1558

Allodi I, Udina E, & Navarro X (2012). Specificity of peripheral nerve regeneration: interactions at the axon level. Prog Neurobiol, 98(1), 16–37. https://doi.org/S0301-0082(12)00072-X [pii]10.1016/j.pneurobio.2012.05.005 [doi] [PubMed: 22609046]

Angeloni NL, Bond CW, Tang Y, Harrington DA, Zhang S, Stupp SI, … Podlasek CA (2011). Regeneration of the cavernous nerve by Sonic hedgehog using aligned peptide amphiphile nanofibers. Biomaterials, 32(4), 1091–1101. https://doi.org/S0142-9612(10)01288-3 [pii]10.1016/j.biomaterials.2010.10.003 [doi] [PubMed: 20971506]

Arslantunali D, Dursun T, Yucel D, Hasirci N, & Hasirci V (2014). Peripheral nerve conduits: technology update. Medical Devices (Auckland, N.Z.), 7, 405–24. https://doi.org/10.2147/MDER.S59124

Bailey SB, Eichler ME, Villadiego A, Rich KM, & Louis S (1993). The influence of fibronectin and laminin during Schwann cell migration and peripheral nerve regeneration through silicon chambers. J Neurocytol, 22(3), 176–184. [PubMed: 8478639]

Banks C, Knox C, Hunter D, Mackinnon S, Hohman M, & Hadlock T (2015). Long-Term Functional Recovery after Facial Nerve Transection and Repair in the Rat. Journal of Reconstructive Microsurgery, 31(3), 210–216. https://doi.org/10.1055/s-0034-1395940 [PubMed: 25629206]

Bell JH, & Haycock JW (2012). Next generation nerve guides: materials, fabrication, growth factors, and cell delivery. Tissue Eng Part B Rev, 18(2), 116–128. https://doi.org/10.1089/ten.TEB.2011.0498 [doi] [PubMed: 22010760]

Berns EJ, Sur S, Pan L, Goldberger JE, Suresh S, Zhang S, Stupp SI (2014). Aligned neurite outgrowth and directed cell migration in self-assembled monodomain gels. Biomaterials, 35(1), 185–195. https://doi.org/S0142-9612(13)01177-0 [pii]10.1016/j.biomaterials.2013.09.077 [doi] [PubMed: 24120048]

Biazar E, Khorasani MT, Montazeri N, Pourshamsian K, Daliri M, Mostafa Rezaei T, Biazar E Montazeri N, Pourshamsian K, Daliri M, Rezaei M, Jabarvand M, Khoshzaban A, Heidari S, Jafarpour M, Roviemiab Z, K. MT (2010). Types of neural guides and using nanotechnology for peripheral nerve reconstruction. International Journal of Nanomedicine, 5(1), 839–852. https://doi.org/10.2147/IJN.S11883 [PubMed: 21042546]

Biglioli F, Colombo V, Tarabbia F, Pedrazzoli M, Battista V, Giovanditto F, Frigerio A (2012). Double innervation in free-flap surgery for long-standing facial paralysis. J Plast Reconstr Aesthet Surg, 65(10), 1343–1349. https://doi.org/S1748-6815(12)00238-0 [pii]10.1016/j.bjps.2012.04.030 [doi] [PubMed: 22728067]

Boahene K (2013). Reanimating the paralyzed face. F1000Prime Reports, 5, 49–5. https://doi.org/10.12703/P5-49 [PubMed: 24273650]

Bond CW, Angeloni NL, Harrington DA, Stupp SI, McKenna KE, & Podlasek CA (2011). Peptide amphiphile nanofiber delivery of sonic hedgehog protein to reduce smooth muscle apoptosis in the penis after cavernous nerve resection. J Sex Med, 8(1), 78–89. https://doi.org/JSM2001 [pii]10.1111/j.1743-6109.2010.02001.x [doi] [PubMed: 20807324]

Brattain K, Medical M, & Consultants T (2013). Analysis of the Peripheral Nerve Repair Market in the United States, 1–11. Retrieved from http://magellanmed.com/wp-content/uploads/2013/09/Analysis-of-the-Peripheral-Nerve-Repair-Market-in-the-US.pdf

Bron LP, & O'Brien CJ (1997). Facial nerve function after parotidectomy. Arch Otolaryngol Head Neck Surg, 123(10), 1091–1096. [PubMed: 9339986]

Byrne PJ, Stuart RM, Fakhry C, Lehar M, & Flint PW (2005). An electrophysiologic model for functional assessment of effects of neurotrophic factors on facial nerve reinnervation. Arch Facial Plast Surg, 7(2), 114–118. https://doi.org/7/2/114 [pii]10.1001/archfaci.7.2.114 [doi] [PubMed: 15781723]

Cao J, Xiao Z, Jin W, Chen B, Meng D, Ding W, Dai J (2013). Induction of rat facial nerve regeneration by functional collagen scaffolds. Biomaterials, 34(4), 1302–1310. https://doi.org/S0142-9612(12)01152-0 [pii]10.1016/j.biomaterials.2012.10.031 [doi] [PubMed: 23122676]

Choe S, Bond CW, Harrington DA, Stupp SI, Kevin T, & Podlasek CA (2018). regeneration and prevent erectile dysfunction, 13(1), 95–101. https://doi.org/10.1016/j.nano.2016.08.032.Peptide

Claudel A, Lazaro RT, Wolfe G, Adams J (2016). Electrophysiological testing and electrical stimulation in neurological rehabilitation neurological rehabilitation Electrophysiological testing. In Umphred's Neurological Rehabilitation (p. Ch 33, 1007–1036).

Daly W, Yao L, Zeugolis D, Windebank A, & Pandit A (2012). A biomaterials approach to peripheral nerve regeneration: bridging the peripheral nerve gap and enhancing functional recovery. J R Soc Interface, 9(67), 202–221. https://doi.org/rsif.2011.0438 [pii]10.1098/rsif.2011.0438 [doi] [PubMed: 22090283]

Davis LA, Gordon TJ, Hoffer JA, Jhamandas J, Stein R (1978). Compound Action Potentials Recorded from Mammalian Peripheral Nerves Following Ligation or Resuturing. J. Physiol, 285, 543–559. [PubMed: 370366]

Flint P et al. (2015). Cummings Otolaryngology Head & Neck Surgery (6th ed.). Elsevier Mosby.

Goodnight JW, Dulguerov P, Berke GS, Lesavoy M, & Hoffman LF (1995). Correlation of compound action potential and electromyography with facial muscle tension. Otolaryngology--Head and Neck Surgery : Official Journal of American Academy of Otolaryngology-Head and Neck Surgery, 112(2), 279–90. Retrieved from http://www.ncbi.nlm.nih.gov/pubmed/7838553 [PubMed: 7838553]

Graber DJ, & Harris BT (2013). Purification and Culture of Spinal Motor Neurons from Rat Embryos. Cold Spring Harbor Protocols, 2013(4), pdb.prot074161-prot074161 https://doi.org/10.1101/pdb.prot074161

Grinsell D, & Keating CP (2014). Peripheral Nerve Reconstruction after Injury: A Review of Clinical and Experimental Therapies. BioMed Research International, 2014 https://doi.org/10.1155/2014/698256

Hadlock TA, Heaton J, Cheney M, & Mackinnon SE (2005). Functional recovery after facial and sciatic nerve crush injury in the rat. Arch Facial Plast Surg, 7(1), 17–20. https://doi.org/7/1/17 [pii]10.1001/archfaci.7.1.17 [doi] [PubMed: 15655169]

Hadlock TA, Kim SW, Weinberg JS, Knox CJ, Hohman MH, & Heaton JT (2013). Quantitative analysis of muscle histologic method in rodent facial nerve injury. JAMA Facial Plastic Surgery, 15(2), 141–6. https://doi.org/10.1001/jamafacial.2013.430 [PubMed: 23329158]

Hadlock TA, Kowaleski J, Lo D, Mackinnon SE, & Heaton JT (2010). Rodent facial nerve recovery after selected lesions and repair techniques. Plast Reconstr Surg, 125(1), 99–109. https://doi.org/10.1097/PRS.0b013e3181c2a5ea [doi]00006534-201001000-00013 [pii] [PubMed: 20048604]

Hadlock TA, Malo JS, Cheney ML, & Henstrom DK (2011). Free gracilis transfer for smile in children: the Massachusetts Eye and Ear Infirmary Experience in excursion and quality-of-life changes. Arch Facial Plast Surg, 13(3), 190–194. https://doi.org/13/3/190 [pii]10.1001/archfacial.2011.29 [doi] [PubMed: 21576665]

Hadlock T. a., Malo JS, Cheney ML, Henstrom DK, GG H, DH H, JK T (2011). Free Gracilis Transfer for Smile in Children. Archives of Facial Plastic Surgery, 13(3), 190 https://doi.org/10.1001/archfacial.2011.29 [PubMed: 21576665]

Hadlock TA, Sundback CA, Hunter DA, Vacanti JP, & Cheney ML (2001). A new artificial nerve graft containing rolled Schwann cell monolayers. Microsurgery, 21(3), 96–101. https://doi.org/10.1002/micr.1016 [pii] [PubMed: 11372069]

Hadlock T, Sheahan T, Heaton J, Sundback C, Mackinnon S, Cheney M, & Article O (2004). Baiting the cross-face nerve graft with temporary hypoglossal hookup. Arch Facial Plast Surg, 6(4), 228–233. https://doi.org/10.1001/archfaci.6.4.228 [doi]6/4/228 [pii] [PubMed: 15262716]

Henstrom D, Hadlock T, Lindsay R, Knox CJ, Malo J, Vakharia KT, & Heaton JT (2012). The convergence of facial nerve branches providing whisker pad motor supply in rats: implications for facial reanimation study. Muscle Nerve, 45(5), 692–697. https://doi.org/10.1002/mus.23232 [doi] [PubMed: 22499096]

Hohman MH, Kleiss IJ, Knox CJ, Weinberg JS, Heaton JT, & Hadlock TA (2014). Functional recovery after facial nerve cable grafting in a rodent model. JAMA Facial Plastic Surgery, 16(1), 20–4. https://doi.org/10.1001/jamafacial.2013.1431 [PubMed: 24232003]

Iseli TA, Harris G, Dean NR, Iseli CE, & Rosenthal EL (2010). Outcomes of static and dynamic facial nerve repair in head and neck cancer. Laryngoscope, 120(3), 478–483. https://doi.org/10.1002/lary.20789 [doi] [PubMed: 20131366]

Jowett N, & Hadlock TA (2015). An Evidence-Based Approach to Facial Reanimation. Facial Plastic Surgery Clinics of North America, 23(3), 313–334. https://doi.org/10.1016/j.fsc.2015.04.005 [PubMed: 26208770]

Kehoe S, Zhang XF, & Boyd D (2012). FDA approved guidance conduits and wraps for peripheral nerve injury: a review of materials and efficacy. Injury, 43(5), 553–572. https://doi.org/S0020-1383(10)00858-2 [pii]10.1016/j.injury.2010.12.030 [doi] [PubMed: 21269624]

Kochhar A, Albathi M, Sharon JD, Ishii LE, Byrne P, & Boahene KD (2016). Transposition of the Intratemporal Facial to Hypoglossal Nerve for Reanimation of the Paralyzed Face. JAMA Facial Plastic Surgery, 18(5), 370 https://doi.org/10.1001/jamafacial.2016.0514 [PubMed: 27348018]

Le Beau JM, Ellisman MH, & Powell HC (1988). Ultrastructural and morphometric analysis of long-term peripheral nerve regeneration through silicone tubes. J Neurocytol, 17(2), 161–172. [PubMed: 3204410]

Li A, Hokugo A, Yalom A, Berns EJ, Stephanopoulos N, Mcclendon MT, Jarrahy R (2014). A bioengineered peripheral nerve construct using aligned peptide amphiphile nanofibers. Biomaterials, 35(31), 8780–8790. https://doi.org/S0142-9612(14)00755-8 [pii]10.1016/j.biomaterials.2014.06.049 [doi] [PubMed: 25064803]

Li A, Hokugo A, Yalom A, Berns EJ, Stephanopoulos N, McClendon MT, Jarrahy R (2014). A bioengineered peripheral nerve construct using aligned peptide amphiphile nanofibers. Biomaterials, 35(31), 8780–8790. https://doi.org/S0142-9612(14)00755-8 [pii]10.1016/j.biomaterials.2014.06.049 [doi] [PubMed: 25064803]

Mattox DE, & Felix H (1987). Surgical anatomy of the rat facial nerve. The American Journal of Otology.

Owusu JA, Truong L, & Kim JC (2016). Facial Nerve Reconstruction With Concurrent Masseteric Nerve Transfer and Cable Grafting. JAMA Facial Plastic Surgery, 18(5), 335 https://doi.org/10.1001/jamafacial.2016.0345 [PubMed: 27197116]

Ridgway JM, Bhama PK, Kim J (2015). Cummings Otolaryngology, Ch 172: Rehabilitation of Facial Paralysis. (P. W. Flint Haughey BH, Lund V, Niparko JK, Robbins KT, Thomas R, Lesperance MM, Ed.) (6th ed.). Elselvier Retrieved from https://www-clinicalkey-com.turing.library.northwestern.edu/#!/content/book/3-s2.0-B978145574696500172X

Shin RH, Friedrich PF, Crum BA, Bishop AT, & Shin AY (2009). Treatment of a segmental nerve defect in the rat with use of bioabsorbable synthetic nerve conduits: a comparison of commercially available conduits. J Bone Joint Surg Am, 91(9), 2194–2204. https://doi.org/91/9/2194 [pii]10.2106/JBJS.H.01301 [doi] [PubMed: 19723997]

Sidle DM, & Fishman AJ (2011). Modification of the orthodromic temporalis tendon transfer technique for reanimation of the paralyzed face. Otolaryngology--Head and Neck Surgery : Official Journal of American Academy of Otolaryngology-Head and Neck Surgery, 145(1), 18–23. https://doi.org/10.1177/0194599811403895 [PubMed: 21493262]

Whitlock EL, Tuffaha SH, Luciano JP, Yan Y, Hunter DA, Magill CK, Borschel GH (2009). Processed allografts and type I collagen conduits for repair of peripheral nerve gaps. Muscle and Nerve, 39(6), 787–799. https://doi.org/10.1002/mus.21220 [PubMed: 19291791]

Zhang S, Greenfield MA, Mata A, Palmer LC, Bitton R, Mantei JR, Stupp SI (2010). A self-assembly pathway to aligned monodomain gels. Nat Mater, 9(7), 594–601. https://doi.org/nmat2778 [pii]10.1038/nmat2778 [doi] [PubMed: 20543836]

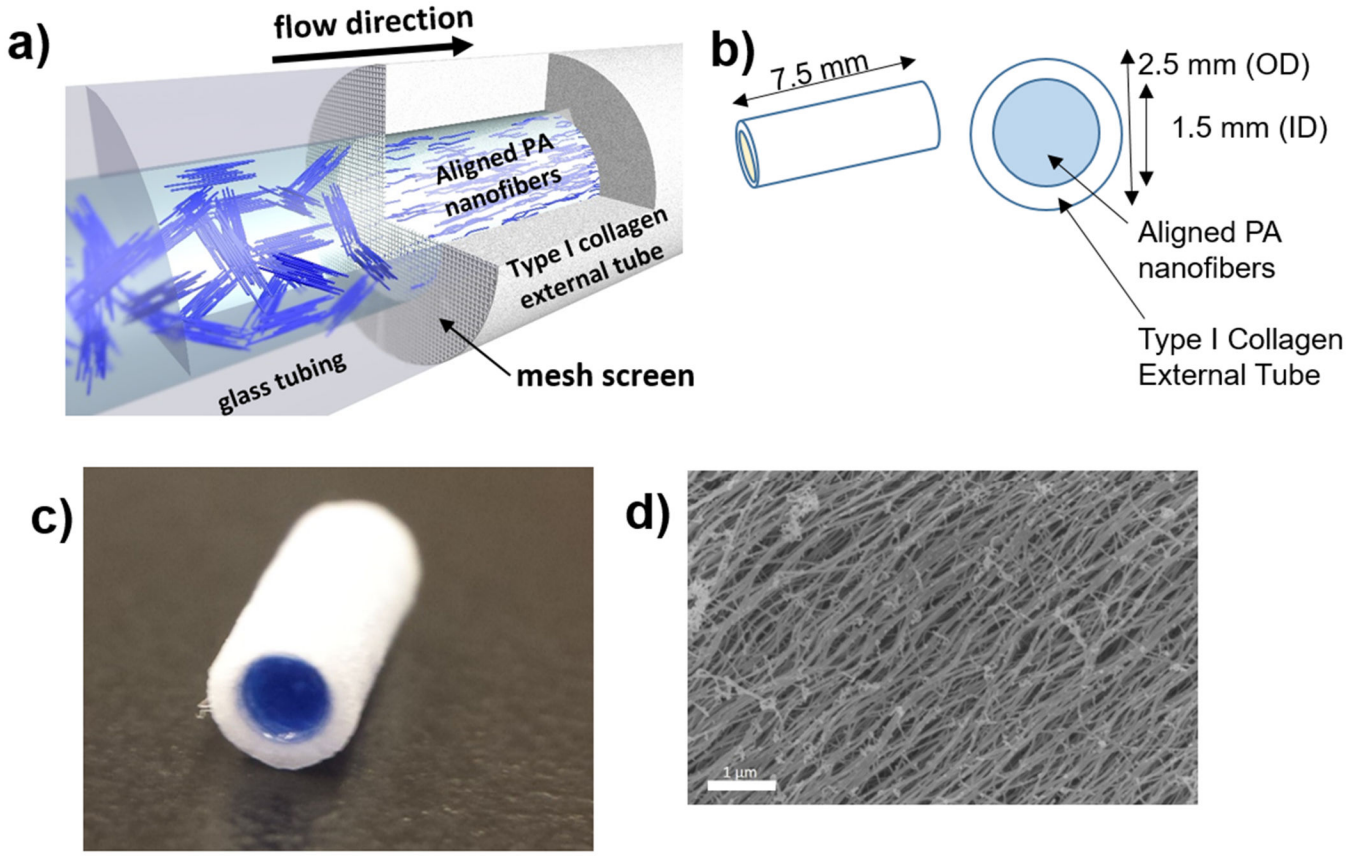

Figure 1.

Aligned nanofiber neurografts were thus constructed: (a) a solution of peptide amphiphile nanofibers is flowed across a mesh screen into the type I collagen external tube, which is then submerged into 25mMol calcium chloride solution to induce gelation, (b) neurograft schematic, OD (outer diameter), ID (inner diameter), (c) macro-photograph of PA nanofiber neurograft, PA nanofiber solution dyed blue for contrast within type I collagen external tube. d) Scanning electron microscopic image of aligned nanofibers within the neurograft, scale bar 1 µm.

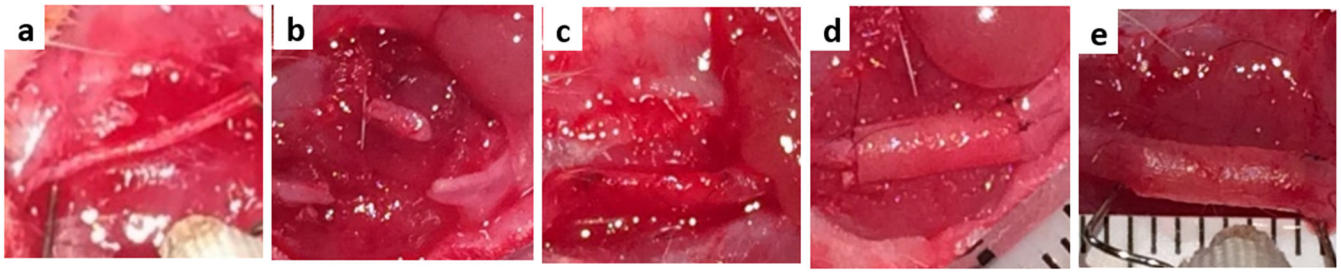

Figure 2. Surgical Photographs of exposed rat facial nerve

a) intact buccal branch of facial nerve elevated by electrodes, b) resected nerve, and c) autograft repair after 8 weeks, neurograft repair d) on day day 0, e) and after 8 weeks, elevated by electrodes.

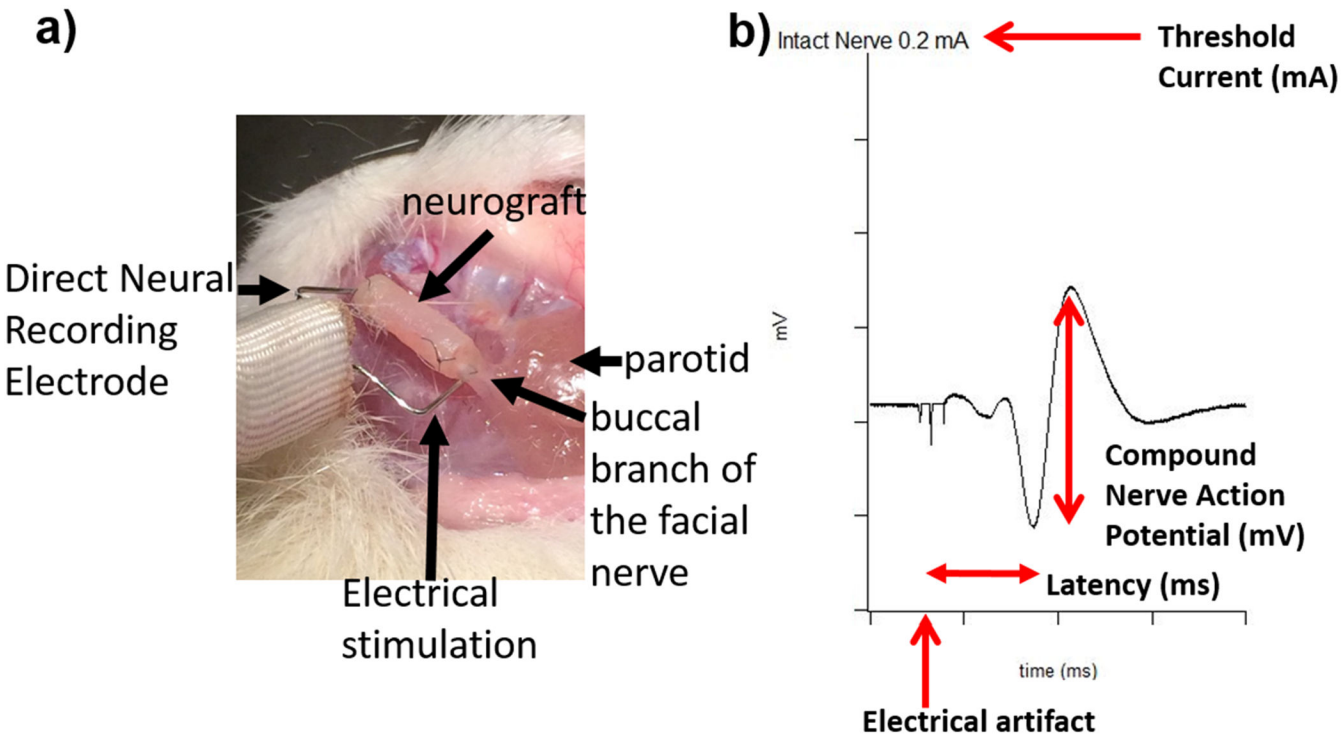

Figure 3.

(a) Photograph of direct neural electrophysiological testing of the buccal branch of the rat facial nerve repaired with the neurograft using a single stimulating and recording electrode. Reference electrodes were placed into the dorsal and limb musculature (not depicted). (b) Sample compound nerve action potential at 0.2 mA electrical stimulus, with maximum peak-to-peak nerve action potential (mV), latency (ms), and electrical artifact depicted.

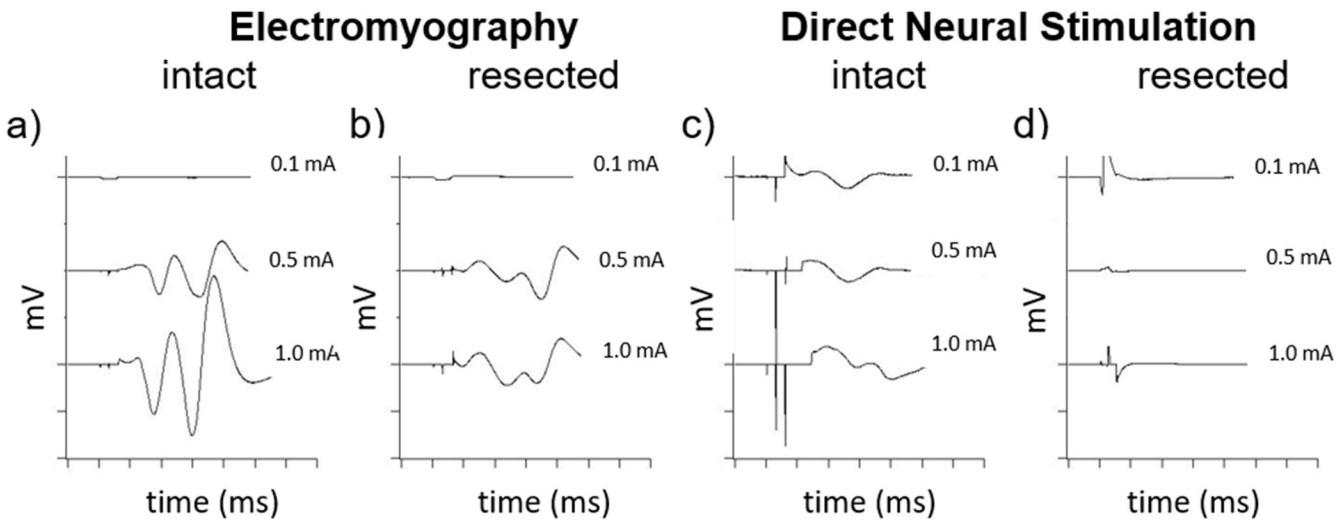

Figure 4. Comparison of Electromyography (EMG) and direct neural stimulation.

EMG compound muscle action potentials (CMAP) of the orbicularis oris muscle after stimulation at the proximal buccal branch of an (a) intact nerve had larger amplitudes but similar threshold currents as (b) 8 weeks after nerve resection, rendering it difficult to distinguish across the range of tested currents (0.1, 0.5, 1.0 mA depicted). Direct neural stimulation more readily distinguished between the (c) intact and (d) resected nerves. The threshold to direct neural stimulation compound nerve action potential (CNAP) for the intact nerve generally occurred by 0.1 mA, whereas the resected nerves after 8 weeks either required a higher current or were electrically silent (d).

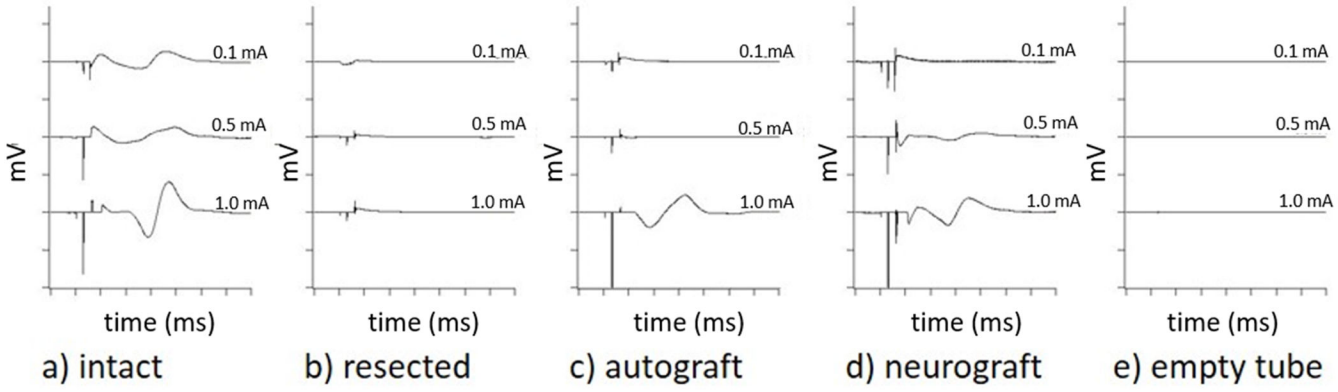

Figure 5. Individual Compound Nerve Action Potentials.

Direct stimulation of nerves with 0.1, 0.5 and 1.0 mA for a) intact nerves, and 8 weeks following b) resection, c) autograft repair, d) neurograft repair, e) repair with empty tube. Vertical axis ticks represent 1 mV, horizontal time axis ticks represent 1 ms. Constant electrical artifact signifies current onset (empty tube electrically silent, electrical artifact present at low mV).

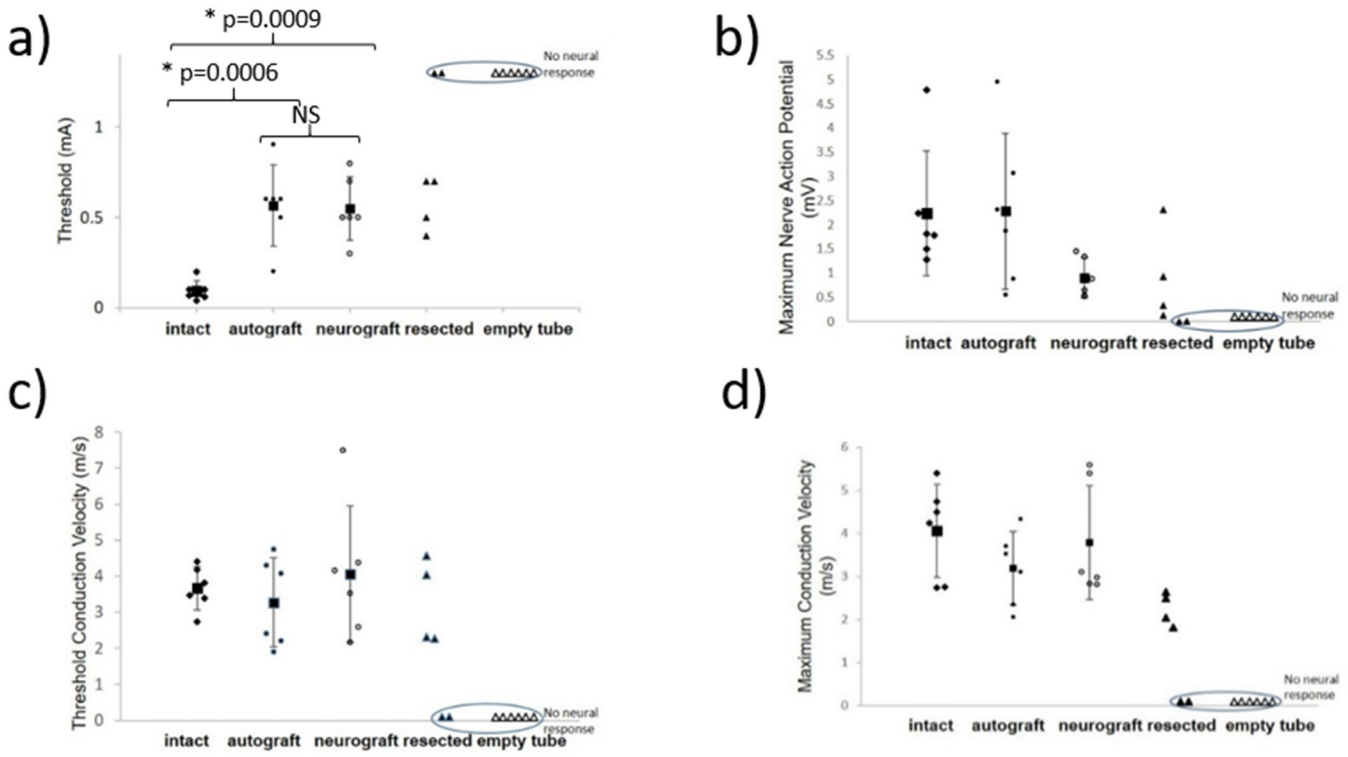

Figure 6.

Electrophysiologic parameters resulting from direct neural stimulation of the intact nerves and 8 weeks following autograft repair, neurograft repair, resection or repair with an empty tube. (a) Intact nerve thresholds were significantly lower at 0.1±0.06 mA than the autograft (0.56±0.2 mA, $p<0.0006$) or neurograft groups (0.55±0.18 mA, $p<0.0009$) (Figure 6a). There was no significant difference in threshold between the autograft and neurograft groups. The facial nerve could be stimulated in four of the rats with resected nerves 8 weeks after the resection albeit at higher threshold currents ranging from 0.4-0.7 mA; in two of the rats the nerves were electrically silent (circled). The empty tube group was electrically silent for all rats (circled). No significant difference between the intact, autograft and neurograft groups was found for the remaining parameters (Figure 6b-d). Each symbol represents an individual rat nerve (N=6 per group) and each square represents the group average with corresponding standard deviations marked.

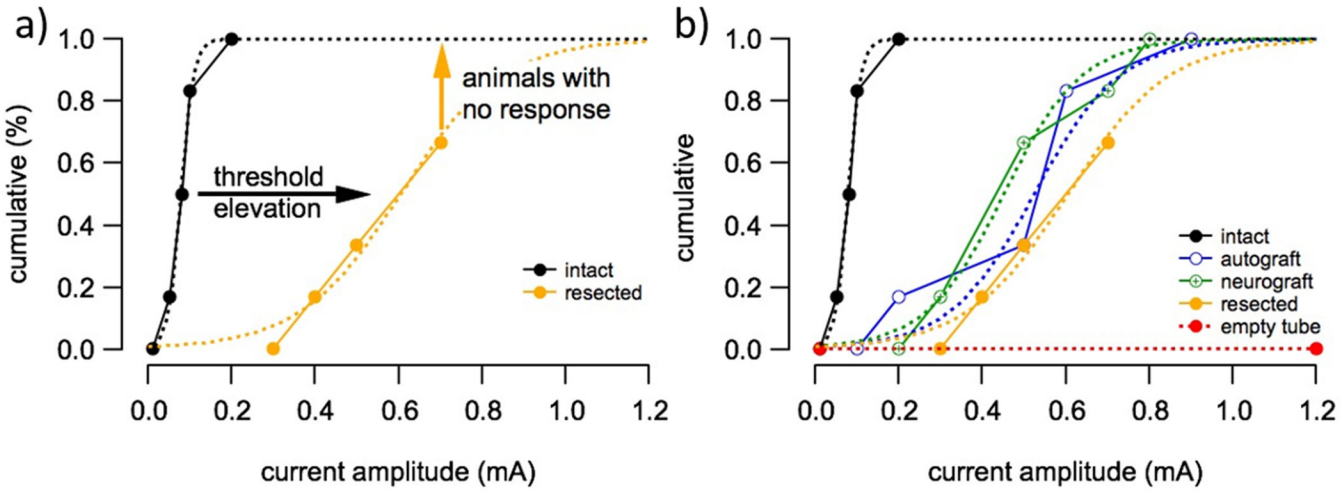

Figure 7. Cumulative percentage of nerve compound action potential (nCAP) across increasing current amplitudes.

(a) The threshold elevation is demonstrated between intact nerves (black line) that upon stimulation produced a nCAP across tested currents compared to resected nerves (orange line), and (b) including the autograft, neurograft and empty tube groups.

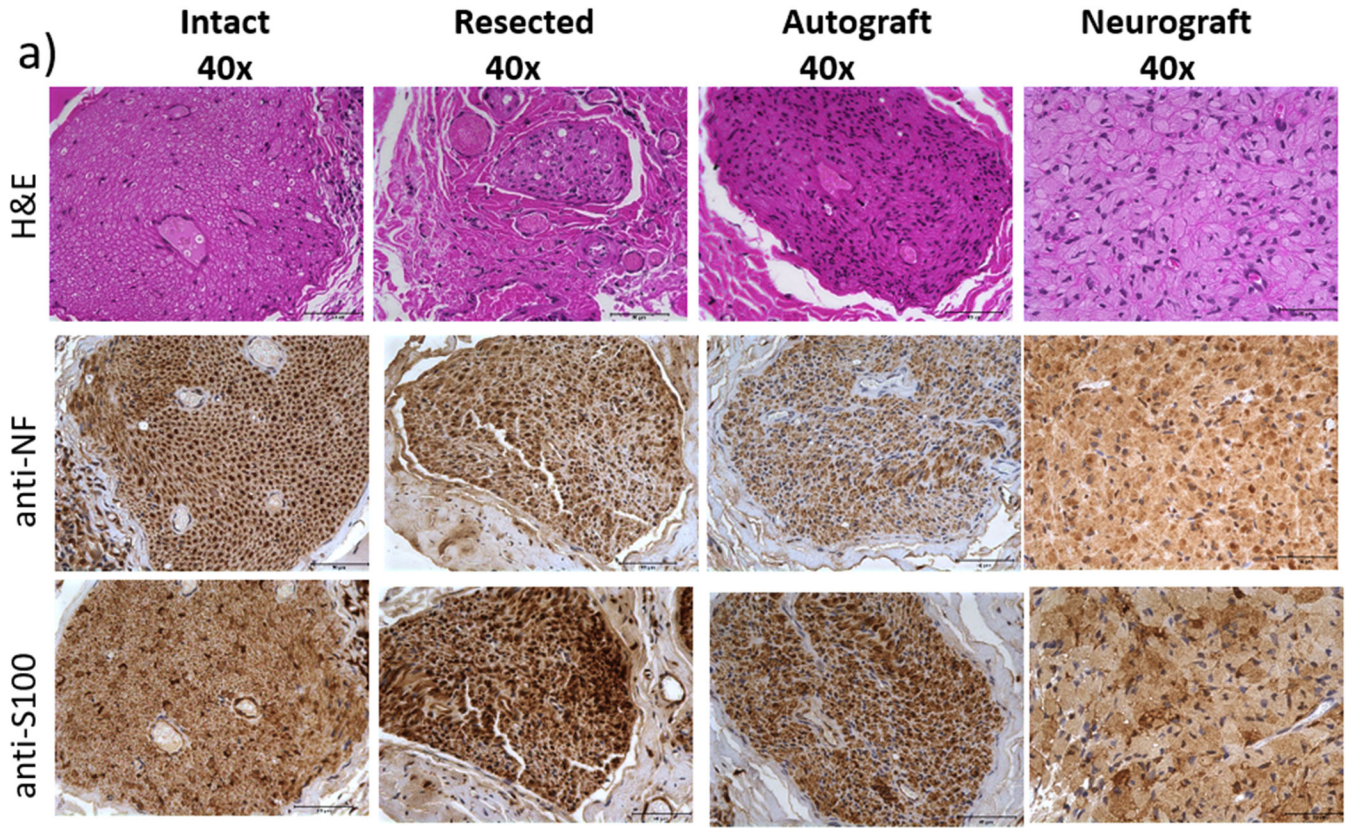

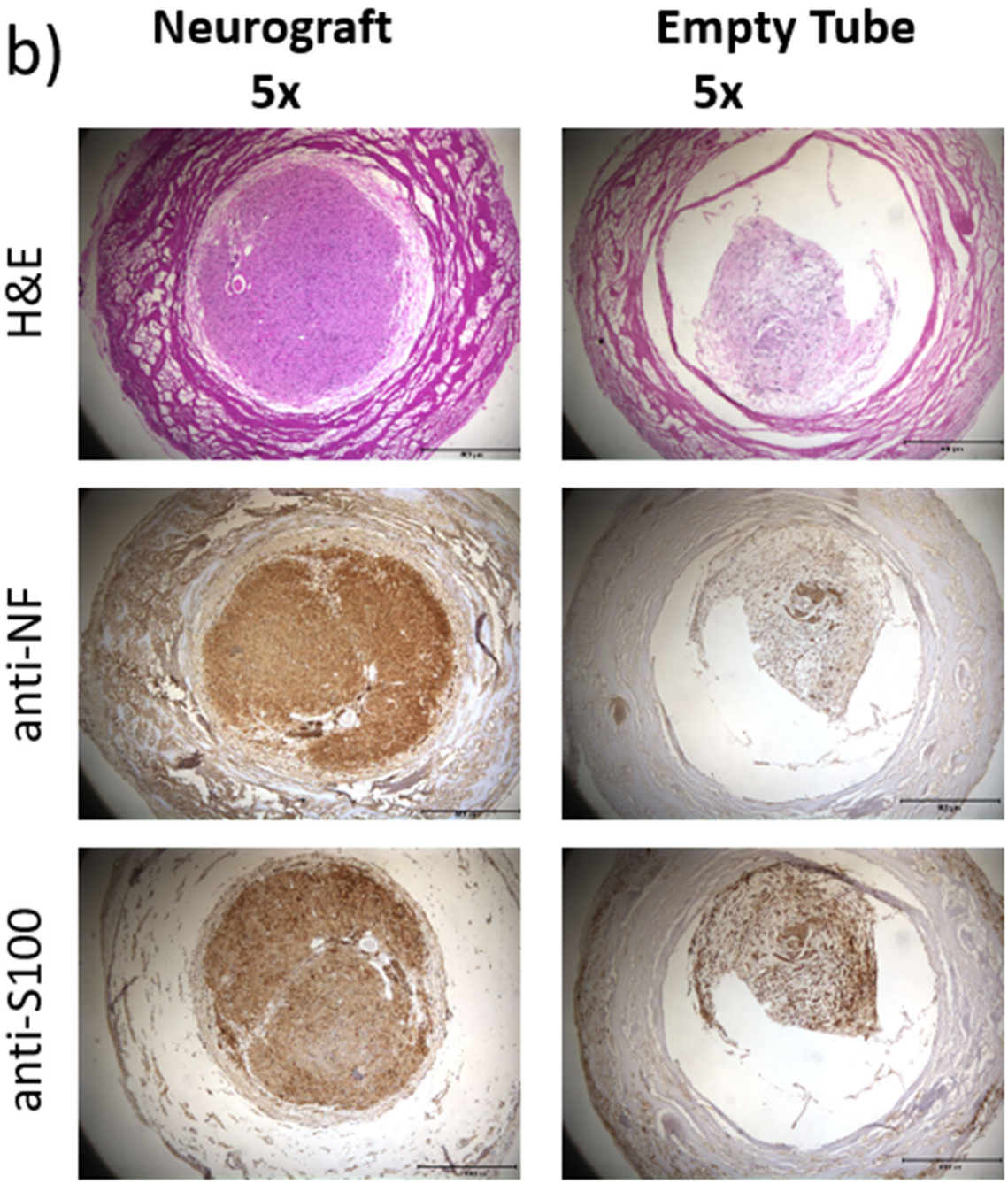

Figure 8. Immunohistochemical analysis of cross sections of (a) the intact nerve, resected nerve distal stump, autograft and neurograft and (b) macorscopic view of entire cross section of neurograft compared with an empty tube.

H&E staining (top), neural tissue phenotype is confirmed with anti-NF (middle) and anti-S100 staining (bottom). Scale bar (a) 50 μm, (b) 500 μm.

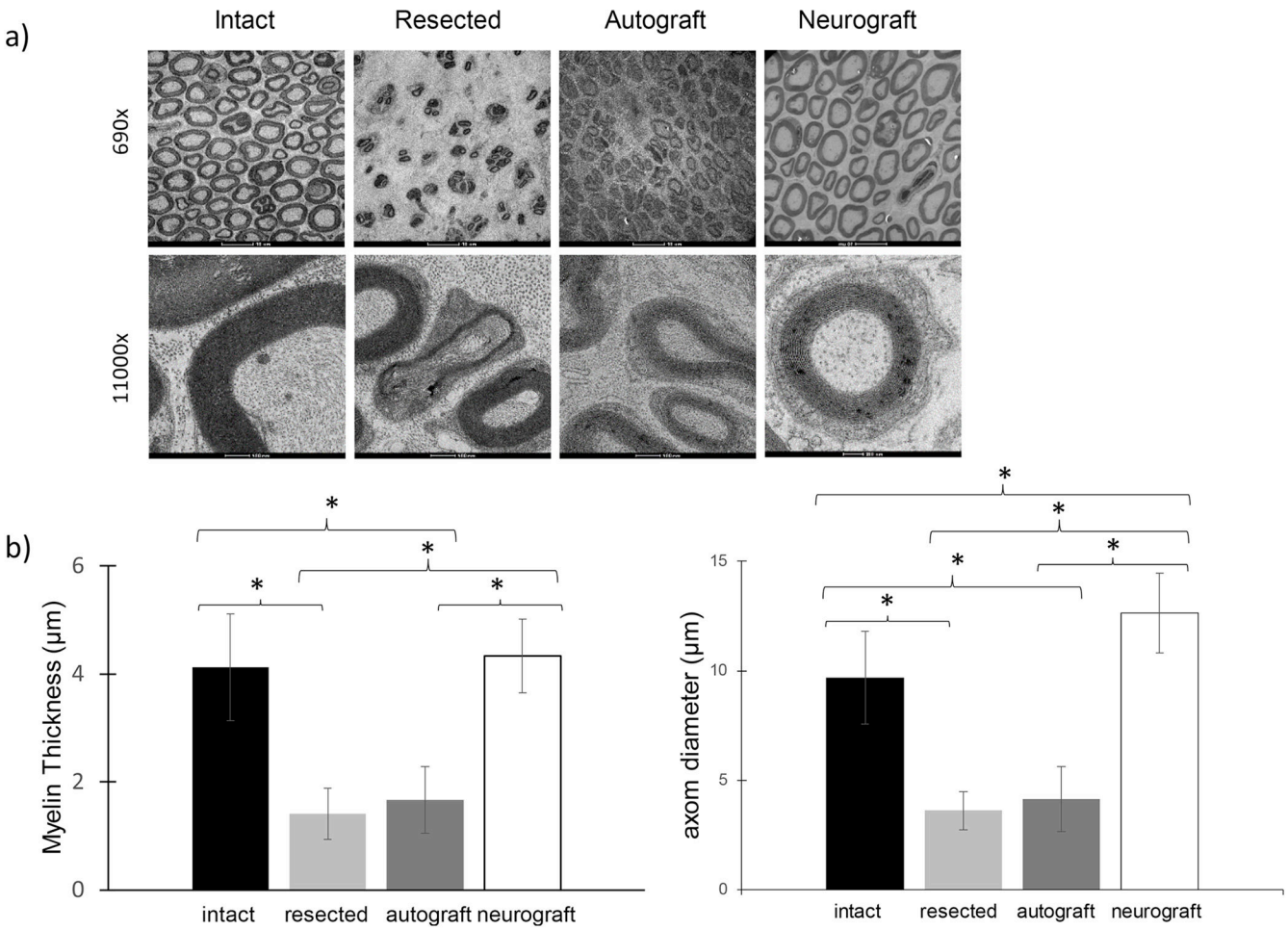

Figure 9.

(a) Transmission electron microscopy (TEM) imaging of cross sections of the intact, resected distal nerve stump, autograft and neurograft are shown (top, scale bar 10 μm). Greater detail of the myelin layers including of the neurograft are shown (bottom, scale bar 200 nm). (b) Average myelin thickness and axon diameter are shown for each group (* indicates statistical significance, $p<0.05$).

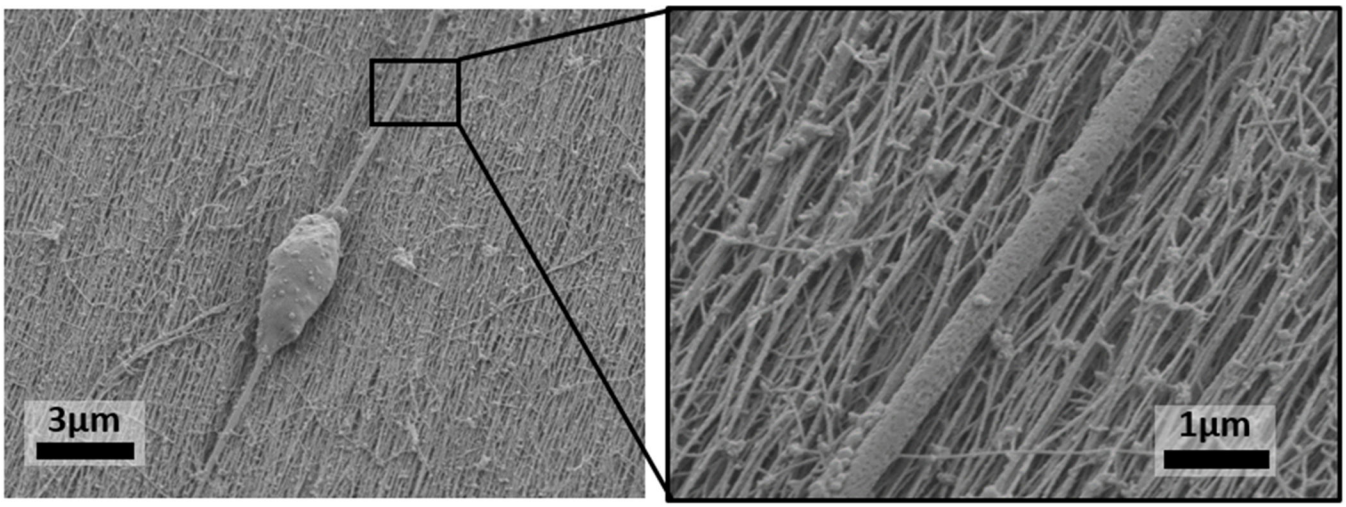

Figure 10. SEM of Motor Neuron Culture

Motor neurons cultured on the surface of aligned PA nanofibers. After 5 days in vitro the majority of axons are seen extending in the direction of nanofiber alignment by contact guidance.